Research Article **AJORR (2022) 5:32**

American Journal of Orthopedic Research and Reviews
(ISSN:2637-4730)

Computational Analysis of Femoral Strength and Fracture Location of Normal, Osteoarthritis and Avascular Necrosis Femurs using CT-Image based Finite Element Method

Zaw Linn Htun[1, 3], Mitsugu Todo[1, 2], Manabu Tsukamoto[4], Takuaki Yamamoto[5], Masaaki Mawatari[6], Yasuharu Nakashima[7]

[1.] Interdisciplinary Graduate School of Engineering Sciences, Kyushu University 6-1 Kasuga-koen, Kasuga 816-8580, Japan; [2.] Research Institute for Applied Mechanics, Kyushu University 6-1 Kasuga-koen, Kasuga 816-8580, Japan; [3.] Department of Physics, University of Yangon, 11041 Kamayut, Yangon, Myanmar; [4.] Department of Orthopaedic Surgery, University of Occupational and Environmental Health, 1-1 Iseigaoka, Yahatanishi-ku, Kitakyushu, Fukuoka 807-8555, Japan; [5.] Department of Orthopedic Surgery, Fukuoka University, 7-45-1 Nanakuma, Jonan-ku, Fukuoka 814-0180; [6.] Department of Orthopedic Surgery, Saga University, 5-1-1 Nabeshima, Saga 849-8501, Japan; [7]Department of Orthopaedic Surgery, Kyushu University 3-1-1 Maidashi, Higashi-ku, Fukuoka 812-8580, Japan

ABSTRACT

Recent years, the risk of hip fractures in elderly people has exponentially increased due to a progressive loss of bone mass and bone structure deterioration due to osteoporosis and increased incidental falls. It is, therefore, expected that the prediction of femoral strength and fracture location of specific patient will be clinically very useful. It is also considered that some typical femoral diseases such as osteoarthritis (OA) and avascular necrosis (AVN) could affect the strength and fracture behaviour of the femurs. In this study, 130 computational femoral models were constructed using CT images of 73 patients. Then, CT image based finite element method (CT-FEM) combined with a damage mechanics analysis was applied to predict the fracture load as the femoral strength and the fracture location of the femoral models. The computational results exhibited that the fracture load tended to increase with increase of the volumetric bone mineral density (vBMD) estimated in the femoral head and neck region in all the three types of models, although AVN models showed much wider scatter in the data than the other two types. The bone fracture behaviour was expressed as expressed as the distribution of failure elements in the head and neck region. The bone fracture mainly took place in the neck region for all types of femoral model. In addition, a combination of the head and neck fracture was also observed in all the models. A combination of neck and intertrochanteric fracture was also observed in the normal and AVN groups.

Keywords: Finite element analysis, Femoral strength, Fracture location, Osteoarthritis, Avascular necrosis, Bone mineral density

***Correspondence to Author:**
Mitsugu Todo[1, 2,]
[1.] Interdisciplinary Graduate School of Engineering Sciences, Kyushu University 6-1 Kasuga-koen, Kasuga 816-8580, Japan; [2.] Research Institute for Applied Mechanics, Kyushu University 6-1 Kasuga-koen, Kasuga 816-8580, Japan;

How to cite this article:
Zaw Linn Htun, Mitsugu Todo, Manabu Tsukamoto, Takuaki Yamamoto, Masaaki Mawatari, Yasuharu Nakashima.Computational Analysis of Femoral Strength and Fracture Location of Normal, Osteoarthritis and Avascular Necrosis Femurs using CT-Image based Finite Element Method .American Journal of Orthopedic Research and Reviews, 2022, 5:32

eSciPub LLC, Houston, TX USA.
Website: https://escipub.com/

1. Introduction

Recent years, the risk of hip fractures in elderly people has exponentially increased due to the degradation of bone structure caused by osteoporosis. Cummings et al. suggested that the number of patients with hip fracture might double or triple by the year 2040 [1]. With the hip fracture incidence increasing worldwide, for each of the osteoporotic patients, the estimation of fracture location and optimum strength of the femur have actively been performed. For example, the bone densitometry and the diagnostic imaging methods have generally been used to predict the risk of bone fracture. These methods usually provide regional bone density values for specific portions of the proximal femur and can visualize figures and shapes of the specific areas of the bone that may be related to the possibility of hip fracture [2]. However, these methods cannot provide a quantitative strength which is directly related to the fracture risk of the femur because the femoral strength depends on its 3D geometry, heterogeneity, distributed mechanical properties, and loading conditions.

In the meantime, a computer simulation method such as the CT-image based finite element method (CT-FEM) has been utilized to estimate the mechanical strength of femurs in order to assess the hip fracture risk of the elderly patient with osteoporosis [3-9]. Moreover, CT FEM can analyse and predict not only the distributions of stress and strain within the bone model but also the fracture locations under the different boundary conditions [9,10].

Along with osteoporosis, some typical femoral diseases such as osteoarthritis (OA) and avascular necrosis (AVN) might significantly affect the femoral fracture behaviour and therefore the femoral strength; however, the effects of such diseases on the mechanical performance of femurs have not been investigated yet. In the present study, 3D computational finite element (FE) models of 130 femurs with healthy, OA and AVN conditions were constructed using CT images of lower limbs of 73 patients. Then, for each of the FE models, the mechanical testing was performed under a compressive loading condition in order to estimate its femoral strength and the fracture behaviour. Such fracture behaviour was recreated as the accumulation of element fracture under both the tensile and compressive stress conditions.

2. Analytical Methods

2.1 Finite Element Modelling

Femoral CT data of 73 patients (10 men aged 37-75 years old, the average age of 51.49 years old; and 63 women aged 19-87 years old, the average age of 65.06 years old) were collected from four different universities hospitals located in the northern Kyushu Island, Japan. From these CT images, a total of 130 computational femoral models were constructed. Based on the patient's clinical data confirmed by orthopaedic surgeons, the 130 femurs were classified into three groups; a normal of 42 femurs (N1 group), OA of 58 femurs (N2 group) and AVN of 30 femurs (N3 group). The three different types of the femur are illustrated in Fig.1.

Three-dimensional numerical and finite element models were constructed using Mechanical Finder v.11 (Research Center of Computational Mechanics Inc., Tokyo, Japan). Firstly, the two-dimensional contours of a femur were extracted from the corresponding CT images, and they were smoothly connected each other to construct three-dimensional femoral model. Then, the inside of the femoral model was filled with the tetrahedral elements to create a finite element (FE) model for the computational mechanical analysis as shown in Fig.2 [11]. The size of the tetrahedral elements was set to 1 to 2 mm. The whole surface of the FE model was also generated using the shell elements to imitate the stiff outer surface of the cortical bone with the greatest bone mineral density [12].

2.2 Mechanical Modelling and Material Properties

The tensile deformation behaviour of all the femoral bone models was assumed to be linear

elastic characterized by two material parameters such as Young's modulus and Poisson's ratio, while their compressive deformation behaviour was assumed to be characterized by an elastic-plastic response with four material parameters such as Young's modulus, Poisson's ratio, yield strength and the work hardening coefficient.

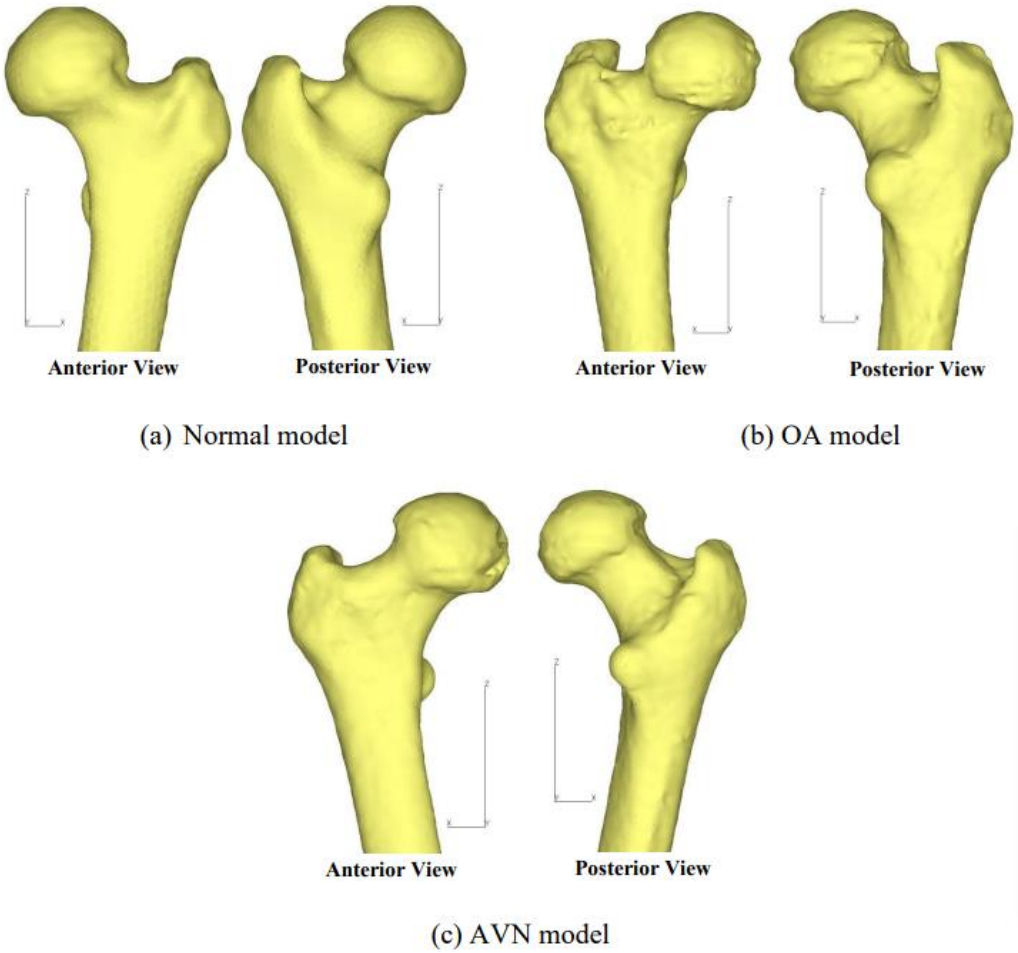

Fig.1: Three different types of femoral models.

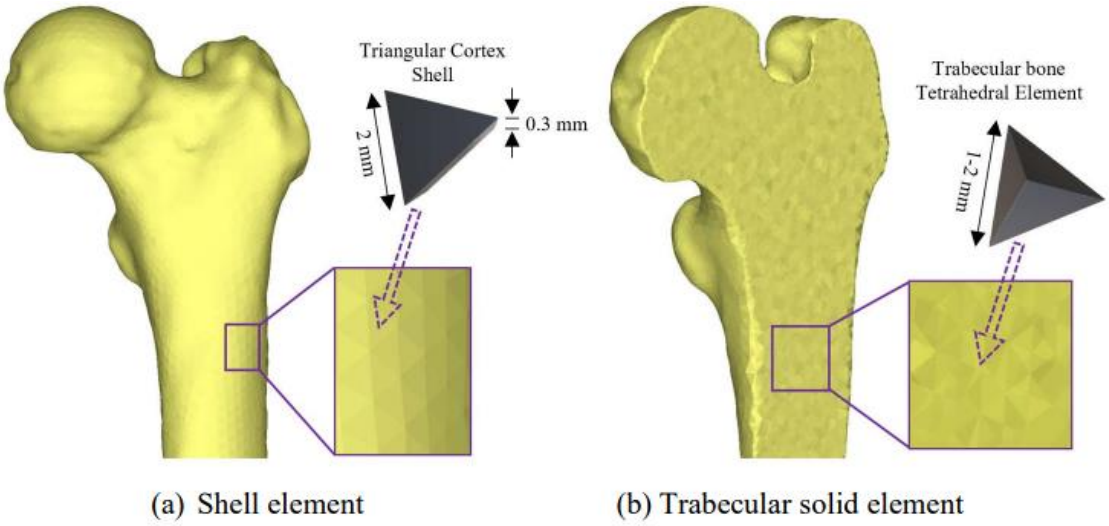

Fig.2: Femoral finite element model. The triangular shell elements were used to model the outer cortex (a), and the trabecular bone and the inner portion of cortical bone were designed using linear tetrahedral elements (b).

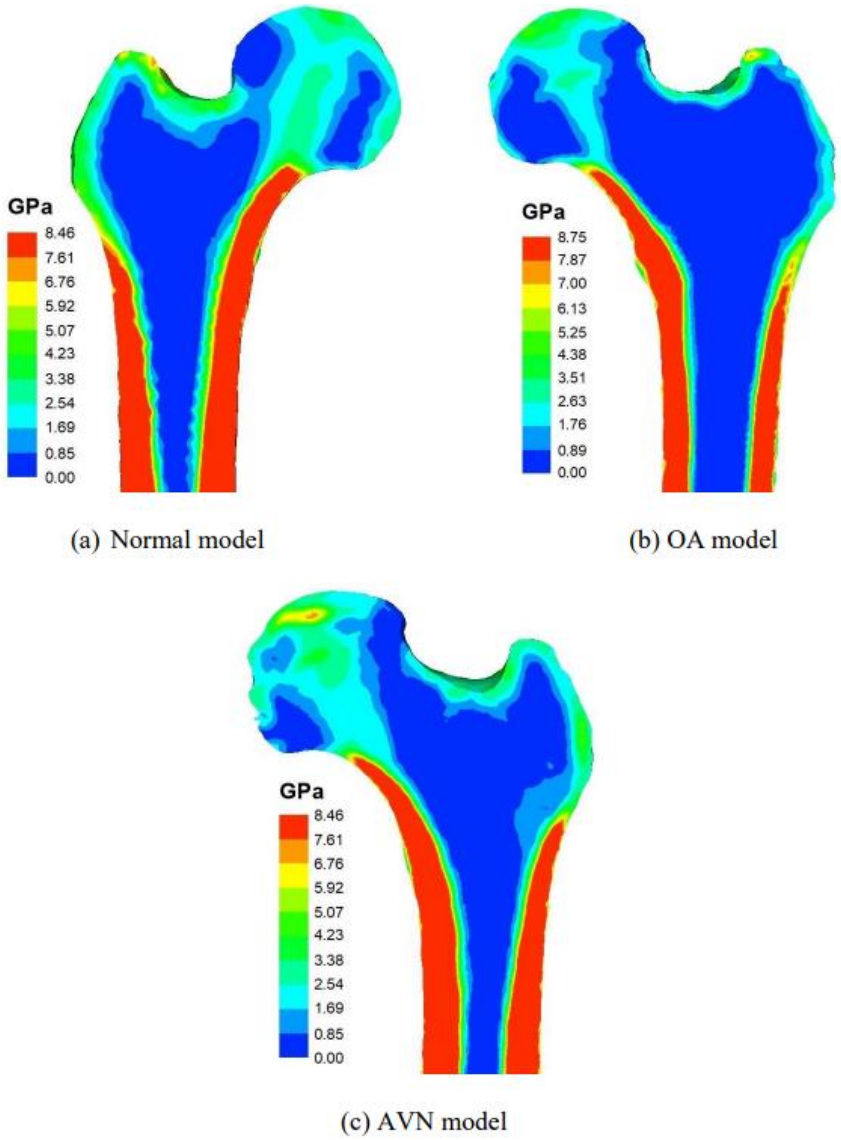

Fig.3: Distribution of Young's modulus in the cross-sectional area.

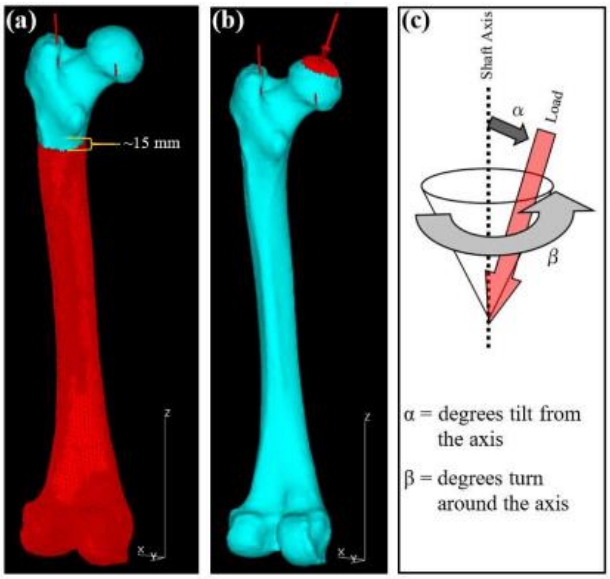

Fig.4: Boundary conditions: (a) fixed condition, (b) loading condition, and (c) angle specification in polar coordinate system to the bone axis.

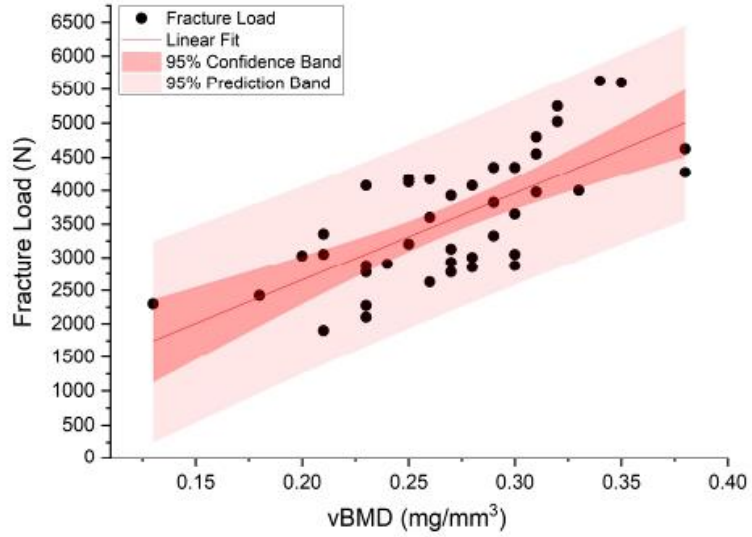

(a) Normal model

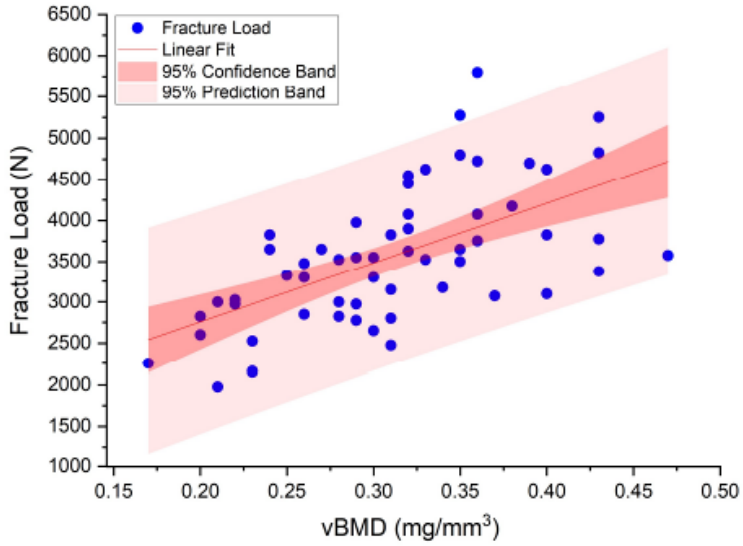

(b) OA model

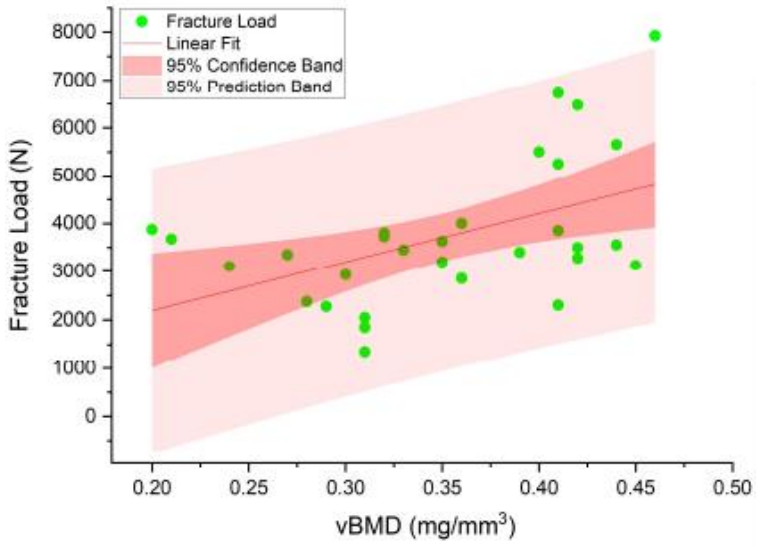

(c) AVN model

Fig.5: Correlation between fracture load and volumetric bone mineral density, including 95% interval of prediction band (pink color) and confidence band (light red color).

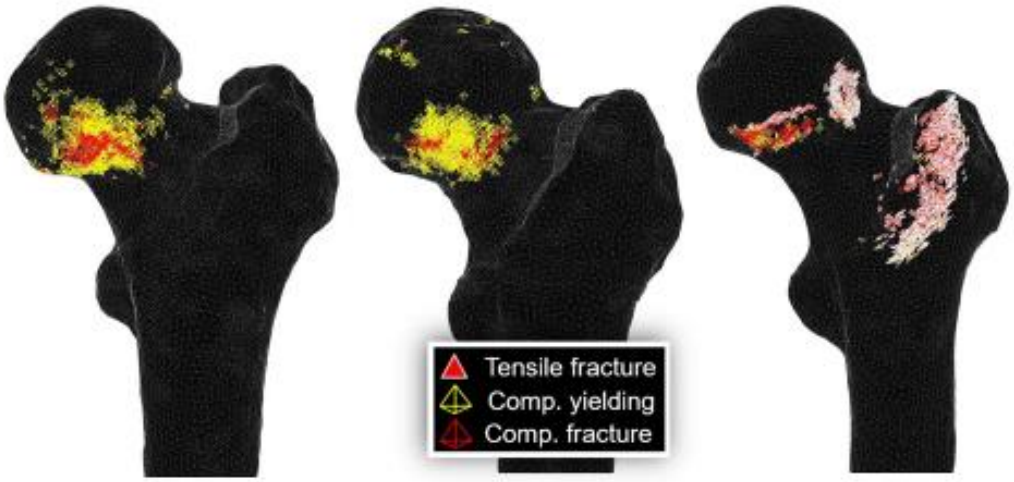

(a) Normal models

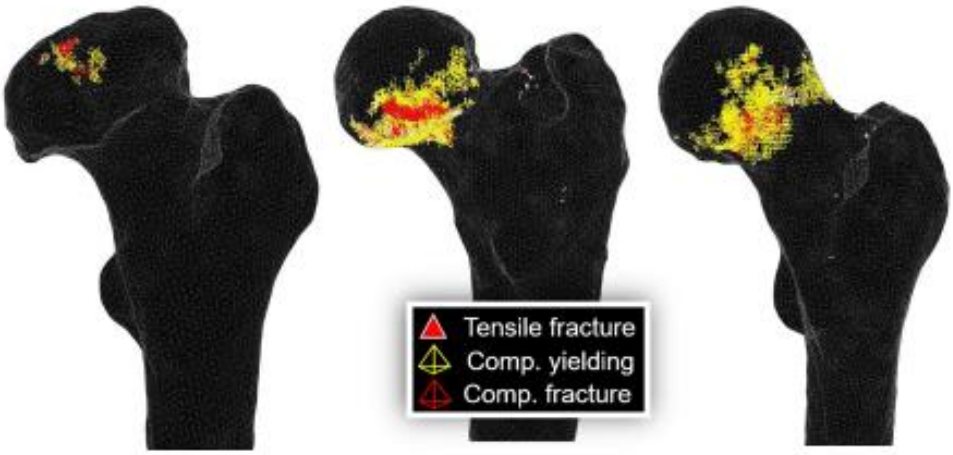

(b) OA models

(c) AVN models

Fig.6: Three different types of bone fracture behaviour. Fracture patterns were expressed as the distribution of failure elements.

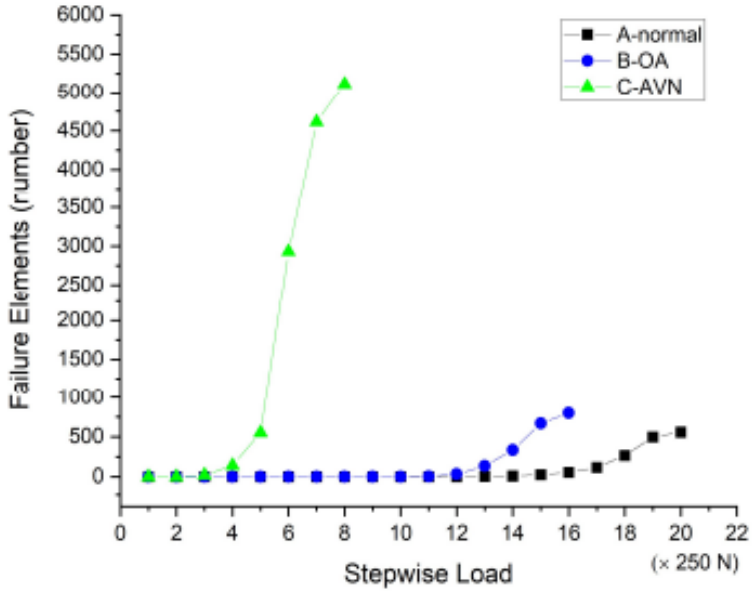

Fig.7: Failure elements against load steps in the three femoral models with the same vBMD.

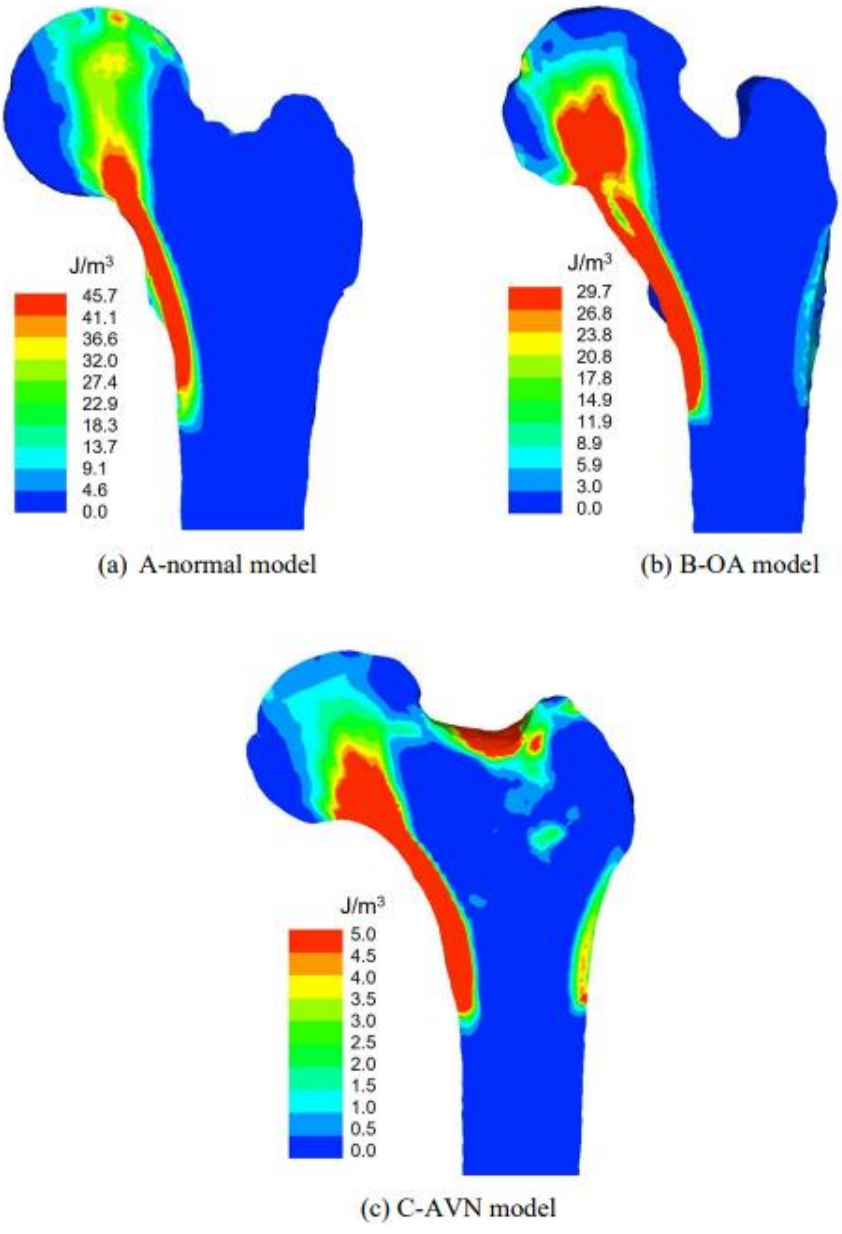

Fig.8 SED distribution patterns of three femoral models with the same vBMD

For each of the tetrahedral elements, its mean bone mineral density (BMD) was firstly calculated from the corresponding CT value (CTv) by using the following linear equation:

$$BMD = 0.001(CTv + 1.4246)/1.0580 \quad (1)$$

where the units of BMD and CTv are given by g/cm^3 and Hounsfield Unit, respectively. Then Young's modulus of the element was estimated from the corresponding BMD by using the empirical formulae proposed by Keyak [13]. For all the tetrahedral elements, Poisson's ratio was set to 0.4 [3]. On the contrary, for all the shell elements, Young's modulus and Poisson's ratio were fixed to 20.6 GPa and 0.167, respectively. The distribution patterns of Young's modulus in the three femoral models presented in Fig.1 are shown in Fig.3. Distribution of the higher moduli corresponded to the location of cortical bone, while the lower moduli expressed cancellous bone and marrow.

Under the compressive deformation of all the elements, it was assumed that the onset of yielding took place when the Drucker-Prager equivalent stress reached the compressive yield strength (this is called 'Drucker-Prager yield criterion'). The yield strength of each element was also obtained from the element's BMD by using the empirical formulae proposed by Keyak [13], while the yield strength of all the shell elements was set to 20.6 MPa. The work hardening coefficient was set to 0.07 for all the elements.

In this FE analysis, bone fracture was reproduced as an aggregation of failure elements. Different failure criterions were used in the tensile and compressive stress conditions. Under the tensile stress condition, the maximum principal stress criterion was utilized to express the onset of tensile bone fracture. It was assumed that the tensile failure of an element took place when the maximum principal stress reached its critical value, which was equal to 0.8 × (compressive yield strength) [9]. On the contrary, under the compressive stress condition, the minimum principal strain criterion was used to express the compressive bone fracture. It was assumed that the compressive failure of an element took place when the minimum principal strain reached its critical value which was equal to -10000u strain, following the yielding of the element [14]. The failure of the element under both tensile and compressive conditions was expressed by reducing the modulus down to the minimum value in the whole femoral model. The strength of the femoral model was then defined as a critical value of the applied load when 15 shell elements were failed [15].

2.3 Boundary Conditions

Firstly, the bone axes were set on the basis of the femoral method and then, the boundary conditions were determined accordingly. The boundary conditions, i.e., the fixed and loading conditions, are shown in Fig.4, respectively. As the fixed condition, the femoral surface from the bottom condylar surface to the line on the diaphysis located approximately 15 mm below the lesser trochanter was totally fixed as shown in Fig.4(a). The distributed load was applied to the top surface of the femoral head under stance configuration as shown in Fig.4(b). The total value of the applied load was set to 10,000 N. The total load was divided into 10 main steps and each of the main steps was also divided into 4 sub-steps. Concerning the loading direction, α was defined as the degree tilt from the longitudinal axis, while β was the degree turn around the axis as shown in Fig.4(c) [13]. In this analysis, α and β were set to 20º and 137 º, respectively.

3. Results and Discussion

3.1 Correlation Between Fracture Load and vBMD

It is well known that an average BMD has a strong correlation with the femoral strength; therefore, in this study, for each of the femoral models, the average volumetric BMD (vBMD) in the femoral head and neck region was obtained. The correlation between the fracture load and vBMD of the normal femurs is shown in Fig.5(a). After a linear regression was fitted on the data, Pearson's correlation coefficient was found to be

r = 0.71, and it could be said that the higher vBMD tended to reuslt in the higher fracture load. Confidience interval (CI) statistics was also performed to precisely estimate the samples' mean. Both of 95% predicted bands and 95% confidence bands of the fitted curve are also shown in Fig.5(a) as well. The statistical results showed that the mean of 95% confidence interval was in a range from 3,308±682 to 3,872±667 N (mean±standard deviation). This implyed that the mean fracture load of all 42 normal models existed within this range with 95% confident.

Similarly, for both the OA and AVN femurs, the correlations between the fracture load and vBMD are shown in Figs.5(b) and (c), respectively. 95% CI means were observed in a range from 3,338±491 to 3,807±501 N for OA models and from 3,053±795 N to 4,414±692 N for AVN models, respectively. The Pearson's *r* values were also found to be 0.60 and 0.49, respectively. In contrast to the normal models, there were two outliers and one outlier from the 95% confidence band of OA and AVN models. These would affect the linear correlation of the fracture load and vBMD, and resulted in lower *r* values. It should be noted that the load range of AVN models was apparently wider than those of the normal and OA models. This fact could be closely related to the peculiar structural and mechanical properties of AVN femurs, depending on their stage and severity such as the extent of crescent percentage of the articular surface and extent of collapsed surface [16]. The AVN femurs used in this study were classified in the 4 stages and therefore, the different stages could result in the broad range of fracture load. It was also to be noteworthy that the maximum value of vBMD of both OA and AVN femurs were significantly higher than that of the normal femur because of the severe deformation of the femoral head. The mean fracture loads of lower and upper 95% confidence interval and their descriptive statistical value for each femur type are listed in Table.1.

Table.1: Mean fracture loads of individual femur group (unit: N)

Types of femur	Data	Mean	Standard Deviation	Minimum	Median	Maximum
Normal	Lower 95% Confidence Interval	3307	682	1125	3362	4510
	Upper 95% Confidence Interval	3872	667	2367	3781	5500
OA	Lower 95% Confidence Interval	3338	491	2136	3385	4280
	Upper 95% Confidence Interval	3807	501	2943	3730	5161
AVN	Lower 95% Confidence Interval	3053	795	1009	3256	3913
	Upper 95% Confidence Interval	4414	692	3373	4251	5711

3.2 Bone Fracture Behaviour

For each femoral model, the compressive fracture behaviour was expressed as the distribution of failure elements in the femoral head and neck region. Three different types of distribution of failure elements are shown for each of the femoral models in Fig.6. Those microdamages consisted of three different failure modes, that is, tensile fracture, compressive yielding, and compressive fracture. The fracture regions were classified into 4 different types as shown in Table 2. It was noted that the bone fracture mainly took place in the neck region (including at least one of subcapital, transcervical and basicervical areas) for all types of femoral model. In addition, a combination of the head and neck fracture was also observed in all the models. Especially, in which OA models showed as many as 16 out of 58 models. Moreover, 10 out of 58 OA models exhibited fractures in their head regions. It was reasonably considered that OA femurs have a higher

fracture risk in the head region compared to the normal and AVN femurs. This might be related to the deformity of the femoral head due to OA. On the other hand, a combination of neck and intertrochanteric fracture was also observed in the normal and AVN groups. This type of fracture highly happened in the AVN femurs (10 out of 30). More importantly, AVN femurs might fracture in all possible locations. It could be due to the variety of AVN stages. It is also to be noteworthy that the AVN femurs with potentially intertrochanteric fracture were mostly with stage 3 and above, whereas head fractured AVN femurs were all stage 4 with serious femoral head collapse.

Table.2: Classification of fracture region

	Fracture Region			
Type of Femur	Head	Neck	Head + Neck	Neck +Intertrochanteric
Normal (N=42)	-	N=36 (86%)	N=3 (7%)	N=3 (7%)
OA (N=58)	N=10 (17.2%)	N=32 (55.2%)	N=16 (27.6%)	-
AVN (N=30)	N=3 (10%)	N=13 (43.4%)	N=4 (13.3%)	N=10 (33.3%)

3.3 Comparison of Fracture Mechanism of Three models with same vBMD

Among all the 130 femoral models, it was found that some of them had the same vBMD with very different fracture load. In order to understand the difference of fracture mechanism, three models denoted by A-normal, B-OA and C-AVN with the same vBMD of 0.31 mg/mm^3 were picked up. The fractue load values of the three models were 4,800, 3,825, and 1,850 N, respectively.

For each of the three models, accumulation of failure elements is shown as a function of load step in Fig.7. One step of load corresponded to 250 N. The strongest model, A-normal, reached up to 20 steps with low number of failure elements (1528), while the weakest model, C-AVN, reached only 8 steps with very large number of failure elements (13367). B-OA model reached 16 steps with the relatively low number of failure elements (1973). Distribution of strain energy density (SED) on the cross-sections of the three models at the fracture load are also shown in Fig.8. In A-normal and B-OA models, it was clearly seen that high SED smoothly distributed from the femoral head to the medial cortical bone, suggesting an ideal propagation of mechanical stress from the top surface of femoral head to the stiff and strong cortical bone and resulting in the high fracture load. On the contrary, in C-AVN model, SED was unnaturally concentrated on the lateral side of neck where BMD and Young's modulus were much lower than the medial side, indicating that neck fracture occurred easily. This unnatural SED concentration was obviously owing to the unique leaning shape of the head and neck region, which caused greater bending moment under the compressive loading, resulting in the localized SED concentration.

4. Conclusions

In this study, normal, OA and AVN femoral FE models were constructed using medical CT images. Then, the fracture load as the patient-specific femoral strength and the fracture location were analyzed by the finite element analysis (FEA) combined with a damage mechanics analysis. The conclusions were obtained as follows:

(1) The fracture load tended to increase with increase of the average vBMD of the head and neck with wide scatters. The Pearson's *r* values of normal, OA and AVN models were evaluated as 0.71, 0.60 and 0.49, respectively, corresponding to the widest scatter observed in AVN models.

(2) The bone fracture behaviour was expressed

as expressed as the distribution of failure elements in the head and neck region. It was noted that the bone fracture mainly took place in the neck region for all types of femoral model. In addition, a combination of the head and neck fracture was also observed in all the models.

(3) A combination of neck and intertrochanteric fracture was also observed in the normal and AVN groups. This type of fracture highly happened in the AVN femurs.

(4) Three models, A-normal, B-OA and C-AVN model, with the same vBMD were compared. C-AVN exhibited the lowest fracture load with the largest number of failure elements generated at the low revel of load. In C-AVN model, SED was unnaturally concentrated on the lateral side of neck where BMD and Young's modulus were much lower than the medial side, indicating that neck fracture occurred easily.

References

[1]. Cummings SR, Rubin SM, Black D. The future of hip fractures in the United States. Numbers, costs, and potential effects of postmenopausal estrogen. Clinical Orthopaedics and Related Research 1990;(252):163–6.

[2]. Lang TF, Keyak JH, Heitz MW, Augat P, Lu Y, Mathur A, Genant HK. Volumetric quantitative computed tomography of the proximal femur: Precision and relation to bone strength. Bone 1997; 21(1): 101–8.

[3]. Keyak JH, Rossi SA, Jones KA, Skinner HB. Prediction of femoral fracture load using automated finite element modeling. Journal of Biomechanics 1998;31(2):125–33.

[4]. Ota T, Yamamoto I, Morita R. Fracture simulation of the femoral bone using the finiteelement method: How a fracture initiates and proceeds. Journal of Bone and Mineral Metabolism 1999;17(2):108–12.

[5]. Cody DD, Gross GJ, J. Hou F, Spencer HJ, Goldstein S a., P. Fyhrie D. Femoral strength is better predicted by finite element models than QCT and DXA. Journal of Biomechanics 1999;32(10):1013–20.

[6]. Keyak JH, Rossi SA, Jones KA, Les CM, Skinner HB. Prediction of fracture location in the proximal femur using finite element models. Medical Engineering and Physics 2001; 23(9):657–64.

[7]. Bessho M, Ohnishi I, Matsuyama J, Matsumoto T, Imai K, Nakamura K. Prediction of strength and strain of the proximal femur by a CT-based finite element method. Journal of Biomechanics 2007; 40(8): 1745–53.

[8]. Gustafsson A, Tognini M, Bengtsson F, Gasser TC, Isaksson H, Grassi L. Subjectspecific FE models of the human femur predict fracture path and bone strength under single-leg-stance loading. Journal of Mechanical Behavior of Biomedical Materials 2021; 113: 104118.

[9]. Abdullah AH, Todo M, Nakashima Y. Prediction of damage formation in hip arthroplasties by finite element analysis using computed tomography images. Medical Engineering and Physics 2017; 44: 8-15.

[10]. Cristofolini L, Schileo E, Juszczyk M, Taddei F, Martelli S, Viceconti M. Mechanical testing of bones: The positive synergy of finite-element models and in vitro experiments. Philosophical Transactions of the Royal Society A: Mathematical, Physical and Engineering Sciences 2010; 368(1920): 2725–63.

[11]. Ulrich D, Van Rietbergen B, Weinans H, Rüegsegger P. Finite element analysis of trabecular bone structure: A comparison of image-based meshing techniques. Journal of Biomechanics 1998; 31(12): 1187–92.

[12]. Dalstra M, Huiskes R, van Erning L. Development and validation of a three-dimensional finite element model of the pelvic bone. Journal of Biomechanical Engineering 1995; 117(3): 272–8.

[13]. Keyak JH, Skinner HB, Fleming JA. Effect of force direction on femoral fracture load for two types of loading conditions. Journal of Orthopaedic Research 2001; 19(4): 539–44.

[14]. Sato T, Yonezawa I, Mitsugu T, Takano H, Kaneko K. Biomechanical effects of implant materials on posterior lumbar interbody fusion: comparison of polyetheretherketone and titanium spacers using finite element analysis and considering bone density. Journal of Biomedical Science and Engineering 2018; 11(4): 45-59.

[15]. Masatoshi O, Kobayashi N, Inaba Y, Choe H, Ike H, Kubota S, Saito T. Mechanical Strength of the Proximal Femur After Arthroscopic Osteochondroplasty for Femoroacetabular Impingement: Finite Element Analysis and 3-Dimensional Image Analysis. Arthroscopy 2018; 34(8): 2377-2386.

[16]. Murphey MD, Roberts CC, Bencardino JT, Appel M, Arnold E, Chang EY, et al. ACR Appropriateness Criteria Osteonecrosis of the Hip. Journal of the American College of Radiology 2016; 13(2): 147–55.